

Structure Design and Solution of Kinematics of Robot Manipulator for 3D Concrete Printing

Václav Záda and Květoslav Belda 

Abstract—In relation to automated 3D concrete construction printing, a structure design of a suitable robot manipulator is presented as well as analytical solutions of related kinematics. The proposed structure has a higher number of degrees of freedom which can significantly increase the dexterity of a robot end-effector carrying a printing head. It should perform a continual motion along complicated large-scale printing trajectories. The related robot kinematics is derived by a novel representation of working layers in the complex plane using exponential functions. It leads to an explicit derivation of kinematic equations. The theoretical results are presented by examples of motion trajectories with typical configurations of the proposed structure.

Note to Practitioners—This paper deals with a design of suitable robot structures for 3D concrete printing. Such concept is determined for on-site printing of residential houses. This area is developing a lot, but without a systematic design of energy-efficient, space-fitting robotic arms. A suitable structure is proposed, including a kinematic description to determine joint coordinates necessary for robot motion control. To ensure continuous energy-balanced motion during a large-scale printing, the redundant links in the structure are also used. Next research tasks focus on trajectory optimisation in complex print profiles.

Index Terms—Robot kinematics, construction industry, printing, redundant systems, robots.

I. INTRODUCTION

USING a suitable mechanical structure is a current challenge in 3D concrete printing [1]–[3]. The common structures are Cartesian, cylindrical, spherical, articulated, gantry (special Cartesian) and SCARA, see Table I. Gantry and SCARA robots are mostly used for their dominant work at one potential energy layer [4]. Cartesian, cylindrical, or spherical structures are less often used due to limited dexterity as well as usual articulated robots for small working range [5], [6]. Gantry, SCARA, cylindrical and spherical structures have a simple construction, but they must stop fully their links during the printing sharp corners and turns [7].

Manuscript received October 25, 2021; accepted November 29, 2021. This article was recommended for publication by Associate Editor C. Yang and Editor K. Saitou upon evaluation of the reviewers' comments. This work was supported by the Project "3D Print in Civil Engineering and Architecture," CZ.02.1.01/0.0/0.0/16_025/0007424, within the European Operational Programme. (Corresponding author: Květoslav Belda.)

Václav Záda is with the Institute of Mechatronics and Engineering Informatics, Faculty of Mechatronics, Informatics and Interdisciplinary Studies, Technical University of Liberec, 461 17 Liberec, Czech Republic (e-mail: vaclav.zada@tul.cz).

Květoslav Belda is with the Department of Adaptive Systems, The Czech Academy of Sciences, Institute of Information Theory and Automation, 180 00 Prague 8, Czech Republic (e-mail: belda@utia.cas.cz).

This article has supplementary material provided by the authors and color versions of one or more figures available at <https://doi.org/10.1109/TASE.2021.3133138>.

Digital Object Identifier 10.1109/TASE.2021.3133138

Besides, the spherical and articulated robots need reconfigurations to keep horizontal printing [8]. It changes the potential energy and thus increases input energy [9].

In 3D concrete printing, there are many projects in which robots are not fully autonomous and depend still on manual guidance [10]. Let us cite two examples: 'The BOD, Building On Demand' [11], [12] and '3D Concrete House Printer' [13]. The first one strives towards full automation by developing robotic 3D printers based on large gantry structures. The second focuses on specific mobile Cartesian manipulators with a motion via linked chains. However, the structure design for 3D printing is neglected in contrast to research on concrete mixtures. Available general solutions [14], [15] do not meet the needs of mass 3D concrete printing with a specific continuous placement and directional orientation of the printing head in the printing process [16], [17].

This paper deals first with a structural design and requirements for printing robots with respect to commonly used kinematic structures. A specific structure is proposed to meet the stated requirements. Possible structure configurations by joint coordinates are sought in order to achieve the required trajectories, determined in advance by architects and builders. The direct and inverse kinematics are addressed using the original approach based on the representation of robot working layers in a complex plane using exponential functions. The main contribution of the paper is the synthesis of unique analytical solutions that are well suited for 3D concrete printing. These solutions, as a specific selection from infinite possibilities, will reduce computation demands in control design [7]. Finally, examples are shown on selected segments of motion trajectories for specific configurations of the designed structure. This paper deals with kinematics. The next paper will be on structure dynamics and control design.

II. ROBOTIC STRUCTURE DESIGN

A. Requirements for 3D Concrete Printing Robots

In addition to printing technology, the design of suitable robot structures is a new challenge in 3D concrete printing. There are two categories that determine requirements on robot structure: *indoor stationary 3D print* including small and large scale printing and *outdoor mobile 3D print* on site focused predominantly on a large scale printing [3]. We address problems of outdoor mobile 3D print that due to more uncertain surrounding conditions represents more complex task in contrast to indoor printing where conditions can be simply controlled. We are based on personal experience and analysis of projects published on the summary site sharing the news and information about the additive manufacturing industry [10].

The large scale mobile 3D print brings specific factors such as weather conditions, space constraints etc. The requirements for a structure design of suitable robot manipulators, capable of the 3D concrete printing under the above factors, can be specified as follows:

- **robot should retain potential energy as much as possible**, the printing head (end effector) moves mainly in horizontal layers, i.e. the retaining saves total input energy
- **most of dynamic effects should take place in the horizontal plane**, i.e. without the influence of gravity
- **robot moving parts should maintain steady kinetic energy during 3D printing**, i.e. it is desirable to maintain the motion of most robot links, even if the end-effector (tool, printing head) has to stop for a short time
- **robot should be folded in necessary, optimally exploited volume (space)**, i.e. the robot can be folded into a small volume for transport or in complicated workspace at printing (the Cartesian structure does not meet this)
- **robot should be resistant to dust by printing**, i.e. it is advisable to prefer rotating links over sliding ones
- **robot range should be big enough**, i.e. expected working radius should be about 5 to 6 meters
- **robot motion should be relatively accurate**, i.e. a motion error (admissible deviation from the reference trajectory) should not exceed 5 millimetres.

These requirements take into account energy consumption to minimize control actions (efficiency of large-scale and time-consuming 3D print); operating conditions to provide simple and feasible transport and maintenance (mobility and robustness); and aspect of purpose to comply with needs of architects and builders (flexibility and dexterity).

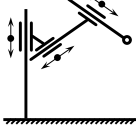
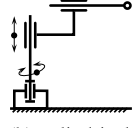
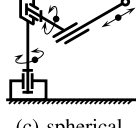
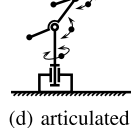
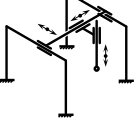
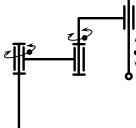
B. Existing Robotic Structures for 3D Concrete Printing

Existing commercial robots, based on conventional structures Cartesian, cylindrical, spherical, articulated (Table I), are usable mainly for indoor printing in limited space. They are characterized by small radius of action, i.e. limited workspace and they are predominantly suitable for printing small components only if consider one stationary robot positions. Furthermore, the existing robots have big energy demands for 3D concrete printing that is based on consecutive construction along horizontal contours in long horizontal layers. Hence, the use of usual commercial robots is inefficient and uneconomical since for long printing, robot drives must move with their links in vertically-different configurations to keep horizontal printing layers and this causes big energy demands more [18]. This statement will be reasoned in section IX. The idea is to move with robot links in horizontal layers predominantly and thus save energy only for kinetic effects like acceleration and deceleration at the beginning and stopping motion and general stationary motion at printing phase.

Remaining variants gantry and SCARA are energy suitable. However, gantry has big requirements on space and initial calibration and SCARA is limited in vertical motion as well as in flexibility in complicated shape environment in relation to civil engineering and construction using 3D print.

Table I summarises the main advantages and disadvantages if mass application of individual robotic structures was considered. For simple tests and individual one-shot automated

TABLE I
CONVENTIONAL ROBOTIC STRUCTURES AND THEIR
PREREQUISITES FOR 3D CONCRETE PRINTING

 <p>(a) Cartesian</p>	<p><i>advantages:</i> adequate workspace; possible keeping one level of potential energy; both indoor/outdoor printing <i>disadvantages:</i> large prismatic joints, transformation of general motion into Cartesian space [19]</p>
 <p>(b) cylindrical</p>	<p><i>advantages:</i> adequate workspace; possible predominant keeping one level of potential energy <i>disadvantages:</i> large prismatic joints, cylindrical workspace [20]</p>
 <p>(c) spherical</p>	<p><i>advantages:</i> predominance of rotational joints – easy protection from dirt [21] <i>disadvantages:</i> changeable level of potential energy; limited spherical workspace; difficult printing head orientation</p>
 <p>(d) articulated</p>	<p><i>advantages:</i> rotational joints only [22] <i>disadvantages:</i> changeable level of potential energy; limited workspace; complicated configuration changing; predominantly for small indoor printing</p>
 <p>(e) gantry</p>	<p><i>advantages:</i> adequate workspace; possible predominant keeping one level of potential energy; suitable for both indoor and outdoor printing [19] <i>disadvantages:</i> occupying a large space</p>
 <p>(f) SCARA</p>	<p><i>advantages:</i> adequate workspace; possible predominant keeping one level of potential energy; suitable for both indoor and outdoor printing <i>disadvantages:</i> complicated configuration changing [23]</p>

constructions, all mentioned structures can be used with regard to the stated features.

C. Designed Robotic Structure

Considering the structures in Table I, option (f) is the closest to meet the above requirements. It retains potential energy and most of its dynamical effects in horizontal arrangement. The structure can be designed for appropriate working radius corresponding to a building site and folded into a relatively small volume. To keep steady kinetic energy, the structure may be extended with another excess link. Although this link will increase complexity of the structure, it will allow the flexible and continuous movement of all links at 3D printing.

A structure that meets the aforementioned requirements is depicted in Fig. 1. The structure is placed in the Cartesian coordinate system (O, x, y, z) with the coordinate subsystem in the horizontal plane (O, x, y) . It is characterized

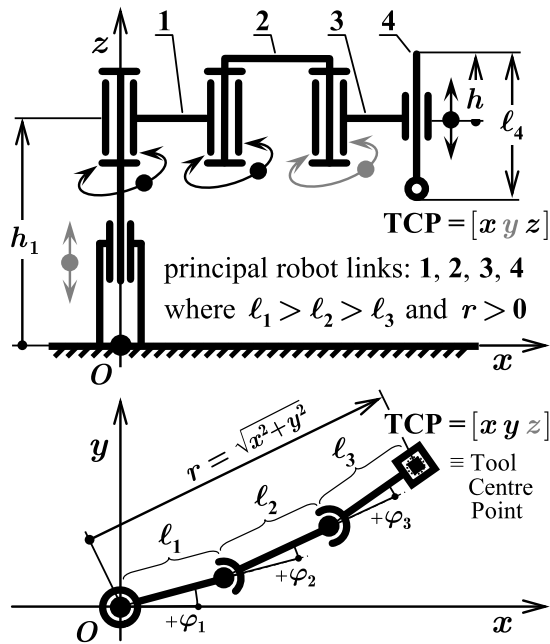


Fig. 1. Dimensional parameters of designed robot structure.

by three main horizontal links with given lengths $l_1 > l_2 > l_3$ and angles φ_1 , φ_2 and φ_3 . The end effector with radius r of the tool center point (TCP) from the origin O has 5 degrees of freedom (DOF). However, only 3 DOF, represented by three revolute joints, and the main horizontal links are significant for motion in printing process.

The remaining 2 DOF serve for the auxiliary vertical linear guiding (two vertical prismatic joints). One of these is placed to the robot base-column. Such a guiding, used in isolated cases only, enables the robot to print in the appropriate vertical ranges, e.g. from zero to half the print height and then to the total height. This joint does not have to be a direct part of the robot, but it can be fully replaced by a vertically extendable platform as a carrier of such a simplified kinematic structure of the robot. This platform can be fully integrated into the vehicle carrying the whole robot and ensuring its fixed position at the place of printing. Hence, the robot can print directly from this vehicle, which moves from one printing location to another if necessary. Finally, the vertical link with printing head ensures regular lifting in compliance with printing stroke.

Thus, the printing robot performs several main movements. Initially, the robot lifts along the base frame column to the desired position and a one layer in the horizontal plane is printed. Then, the printing head together with vertical link is raised up approximately by the layer thickness and the second layer is printed, etc. After printing several layers, the robot is moved up along the base-column again and the whole cycle is repeated. It can be seen from the robot construction and operation that its kinematics can be divided into two separate cases:

- i) the vertical displacement of the entire device or just the last robot link;
- ii) the planar movement of the robot structure in the horizontal plane.

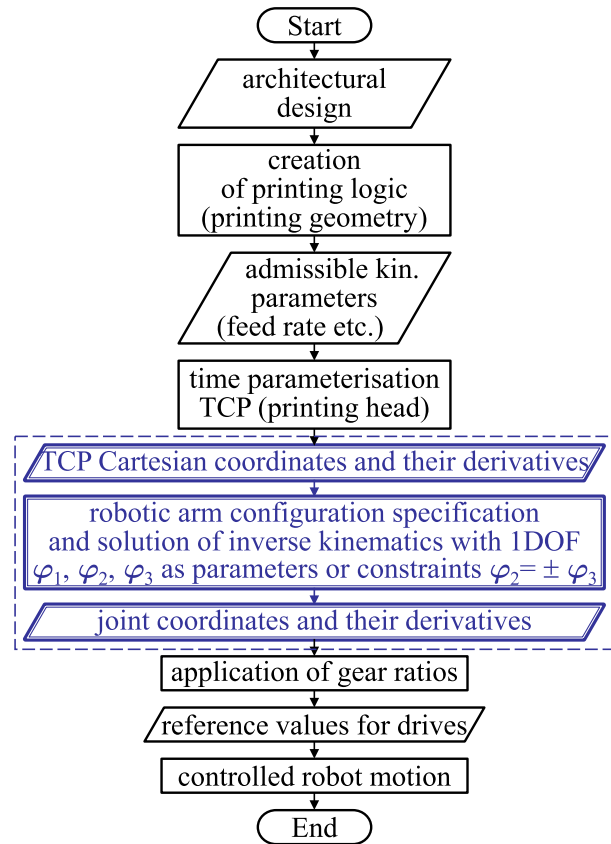


Fig. 2. Flow chart of robot motion trajectory construction.

The first case is completely trivial, but the second one not. However, the movement in the horizontal plane is crucial for the given printing. The following sections explain principles and unique solutions of the kinematic problems, necessary for a design and realisation of the motion by the structure. Specifically, solved issue is indicated in Fig. 2.

D. Structure Design Summary

Proposed robot structure is space-saving, ready for mobile car solutions for outdoor 3D concrete printing. Regarding to the SCARA configuration, it can represent SCARA type structure with variable adjustable link length when specific joint is locked with advance of cranked link where just centre joint is locked enabling robot to turn around the corner or obstacle. Two translational degrees are important, since the first placed to the main column is for one shot or only sparse motion to set range of printing, e.g. from ground to half of printed wall and then to whole height of wall and the second integrated with printing head to move up according to current printed layer.

III. BASIC KINEMATIC PROBLEMS

A. Direct Kinematic Problem

As it was mentioned before, the direct problem of the given structure is easy to solve. It is divided into two subtasks:

- 1) subtask in the xy -plane (horizontal plane);
- 2) subtask in the z -axis (vertical direction).

In the horizontal plane, the coordinates x and y hold

$$x = \ell_1 \cos \varphi_1 + \ell_2 \cos(\varphi_1 + \varphi_2) + \ell_3 \cos(\varphi_1 + \varphi_2 + \varphi_3) \quad (1)$$

$$y = \ell_1 \sin \varphi_1 + \ell_2 \sin(\varphi_1 + \varphi_2) + \ell_3 \sin(\varphi_1 + \varphi_2 + \varphi_3) \quad (2)$$

$$\varphi_{j,\min} \leq \varphi_j \leq \varphi_{j,\max}, \quad j = 1, 2, 3.$$

The coordinates x , y and φ_j may be parameterized by time or curve length. Thus the direct problem is only a simple substitute of the joint angles into equations (1) and (2) and calculate the appropriate values x and y .

Note that the vertical coordinate z holds

$$z = h_1 - l_4 + h, \quad (3)$$

where h_1 is a vertical position of the robot arm along base robot column, and h is a relative stroke with respect to a number of printed layers of concrete bead. The links 1, 2, 3 do not change vertical positions during the print of one layer.

B. Inverse Kinematic Problem

Equations (1) and (2) may be written as a mapping $F : \Omega \rightarrow R^2$, where $\Omega \subset R^3$ is the domain of F . There is no inverse map for F , since a corresponding Jacobian matrix is 2×3 . The problem is ‘‘how to solve the system of singular equations (deficient number of equations) in the problem of inverse task’’, i.e. $\varphi_j = f(x, y)$, $j = 1, 2, 3$. An arbitrary point in the xy -plane has two degrees of freedom (DOF). The area of motion is described by three angles φ_1 , φ_2 , and φ_3 . In principle, there are three possible options here:

- 1) select one angle as a parameter, variable during motion, and calculate the remaining two angles (sec. V);
- 2) choose a fixed mathematical constraint among the angles φ_1 , φ_2 , and φ_3 , to get another equation (sec. VI);
- 3) determine the angles φ_1 , φ_2 , and φ_3 as an optimisation problem for a specifically chosen criterion.

In this paper, we focus on the first two straightforward options. Since a solution of the inverse kinematic problem takes place in the xy -plane, let us transform this problem into one on a complex plane [24], [25]. It will significantly simplify a further derivation of the inverse problem [26].

IV. BASIC RELATIONS FOR FURTHER DERIVATION

This section deals with the determining the angles φ_1 , φ_2 and φ_3 , when one angle selected as a changeable parameter is known and predefined and the remaining two angles have to be determined with respect to it. Even if the all respective angles were given, e.g. by optimisation with specific criterion, the further proposed expressions stay valid.

Let us define a complex variable ζ and its conjugate $\bar{\zeta}$

$$\zeta = x + iy, \quad \bar{\zeta} = x - iy \quad (4)$$

If the well-known Euler formula [25] is used, then

$$\zeta = |\zeta| e^{i\varphi} = |\zeta| (\cos \varphi + i \sin \varphi) \quad (5)$$

applies to an arbitrary angle φ . With these relationships, equations (1) and (2) can be rewritten into a basic equation:

$$\zeta = \ell_1 e^{i\varphi_1} + \ell_2 e^{i(\varphi_1 + \varphi_2)} + \ell_3 e^{i(\varphi_1 + \varphi_2 + \varphi_3)}. \quad (6)$$

It will be used to exclude of particular angles. This is the basis of inverse problem solutions for the designed robot structure.

A. Elimination of Angle φ_1

Equation (6) can be rewritten as follows

$$\zeta = e^{i\varphi_1} (\ell_1 + \ell_2 e^{i\varphi_2} + \ell_3 e^{i(\varphi_2 + \varphi_3)}) \quad (7)$$

$$\bar{\zeta} = e^{-i\varphi_1} (\ell_1 + \ell_2 e^{-i\varphi_2} + \ell_3 e^{-i(\varphi_2 + \varphi_3)}), \quad (8)$$

i.e. the complex variable ζ and its conjugate $\bar{\zeta}$. Since the square of the absolute value of ζ can be written as

$$|\zeta|^2 = \zeta \bar{\zeta} = x^2 + y^2 = r^2, \quad (9)$$

where x and y are the Cartesian coordinates and r is a distance of TCP from the origin O . Then, by mutual multiplying of (7) and (8), the following expression can be obtained

$$r^2 = \ell_1^2 + \ell_2^2 + \ell_3^2 + 2[\ell_1 \ell_2 \cos \varphi_2 + \ell_1 \ell_3 \cos(\varphi_2 + \varphi_3) + \ell_2 \ell_3 \cos \varphi_3] \quad (10)$$

Thus, in this equation, angle φ_1 is eliminated.

B. Elimination of Angle φ_2

Let (6) be written in a different way, as follows

$$\zeta e^{-i\varphi_1} - \ell_1 = e^{i\varphi_2} (\ell_2 + \ell_3 e^{i\varphi_3}) \quad (11)$$

$$\bar{\zeta} e^{i\varphi_1} - \ell_1 = e^{-i\varphi_2} (\ell_2 + \ell_3 e^{-i\varphi_3}). \quad (12)$$

A multiplication of (11) and (12) is as follows:

$$r^2 - 2\ell_1(x \cos \varphi_1 + y \sin \varphi_1) + \ell_1^2 = \ell_2^2 + \ell_3^2 + 2\ell_2 \ell_3 \cos \varphi_3 \quad (13)$$

In this equation, angle φ_2 is eliminated.

C. Elimination of Angle φ_3

In similar way, to eliminate angle φ_3 , the equation (6) can be written in the form

$$(\zeta e^{-i\varphi_1} - \ell_1) e^{-i\varphi_2} - \ell_2 = \ell_3 e^{i\varphi_3} \quad (14)$$

and its complex conjugate as well

$$(\bar{\zeta} e^{i\varphi_1} - \ell_1) e^{i\varphi_2} - \ell_2 = \ell_3 e^{-i\varphi_3}. \quad (15)$$

By mutual multiplication of these two equations, the following expression is obtained

$$\begin{aligned} & (x \cos \varphi_1 + y \sin \varphi_1 - \ell_1)^2 + (y \cos \varphi_1 - x \sin \varphi_1)^2 \\ & - 2\ell_2 [(x \cos \varphi_1 + y \sin \varphi_1 - \ell_1) \cos \varphi_2 \\ & + (y \cos \varphi_1 - x \sin \varphi_1) \sin \varphi_2] = \ell_3^2 - \ell_2^2. \end{aligned} \quad (16)$$

In this equation, angle φ_3 is eliminated.

Equations (10), (13) and (16) will be used in further explanation of the solutions of the inverse kinematic problem. The individually excluded angles, selected as parameters, mean still 1 DOF in the robot arm motion usable for specific user requirements as robot reconfiguration by related links.

V. SELECTION OF VARIABLES φ_i AS PARAMETERS

A. Computation of φ_2 and φ_3 as Functions of φ_1

For the computation, let us consider (16) and define new auxiliary variables $a \geq 0$ and α to simplify it, as:

$$\begin{aligned} x \cos \varphi_1 + y \sin \varphi_1 - \ell_1 &= a \cos \alpha \\ y \cos \varphi_1 - x \sin \varphi_1 &= a \sin \alpha \end{aligned} \quad (17)$$

Hence, based on (17), the following expression is valid:

$$a = \sqrt{(x \cos \varphi_1 + y \sin \varphi_1 - \ell_1)^2 + (y \cos \varphi_1 - x \sin \varphi_1)^2}, \quad (18)$$

where $a > 0$ but $x = \ell_1 \cos \varphi_1$ and $y = \ell_1 \sin \varphi_1$. However, it cannot occur since $\ell_2 > \ell_3$, i.e. in (17), $a > 0$ holds always. Then, it may be computed

$$\cos \alpha = (x \cos \varphi_1 + y \sin \varphi_1 - \ell_1)/a \quad (19)$$

$$\sin \alpha = (y \cos \varphi_1 - x \sin \varphi_1)/a. \quad (20)$$

Here, there is only one angle α such that (19) and (20) hold. Now, relation (16) can be written as

$$a^2 - 2 \ell_2 a \cos(\varphi_2 - \alpha) = \ell_3^2 - \ell_2^2 \quad (21)$$

and hence we obtain

$$\cos(\varphi_2 - \alpha) = (a^2 - \ell_3^2 + \ell_2^2)/(2 \ell_2 a). \quad (22)$$

If we substitute $\delta = \varphi_2 - \alpha$ into this equation we obtain two solutions δ_I, δ_{II} for δ . Thus, there are also two angles φ_2 , i.e. $\varphi_{2,I} = \alpha + \delta_I$ and $\varphi_{2,II} = \alpha + \delta_{II}$. Now, angle φ_3 can be computed directly from equation (13):

$$\cos \varphi_3 = [r^2 - 2 \ell_1 (x \cos \varphi_1 + y \sin \varphi_1) + \ell_1^2 - \ell_2^2 - \ell_3^2]/(2 \ell_2 \ell_3). \quad (23)$$

This equation has two solutions $\varphi_{3,I}$ and $\varphi_{3,II}$, as in the previous case. In full generality, we have two options for φ_2 and two options for φ_3 , i.e. in total the fourth options. Each pair of options for φ_2 and φ_3 must be evaluated to see if they meet the constraints for each angle.

B. Computation of φ_1 and φ_3 as Functions of φ_2

To determine φ_1 and φ_3 as functions of φ_2 , let the expression (16) be written as follows

$$\begin{aligned} 2 \cos \varphi_1 (\ell_1 x + \ell_2 x \cos \varphi_2 + \ell_2 y \sin \varphi_2) \\ + 2 \sin \varphi_1 (\ell_1 y + \ell_2 y \cos \varphi_2 - \ell_2 x \sin \varphi_2) \\ = r^2 + \ell_1^2 + \ell_2^2 - \ell_3^2 + 2 \ell_1 \ell_2 \cos \varphi_2 \end{aligned} \quad (24)$$

Now, let us define auxiliary variables b and β_1 , such that

$$\begin{aligned} \ell_1 x + \ell_2 x \cos \varphi_2 + \ell_2 y \sin \varphi_2 &= r b \cos \beta_1 \\ \ell_1 y + \ell_2 y \cos \varphi_2 - \ell_2 x \sin \varphi_2 &= r b \sin \beta_1 \end{aligned} \quad (25)$$

Then, the value of variable b can be expressed as follows

$$b = \sqrt{\ell_1^2 + \ell_2^2 + 2 \ell_1 \ell_2 \cos \varphi_2} > 0 \text{ since } \ell_1 \neq \ell_2 \quad (26)$$

Thus, for $\varphi_2 \neq \pm\pi$ and $r > 0$, there exists only one unique angle β_1 , which can be computed from (25). Then, from (24), the equation for φ_1 can be derived as follows

$$\cos(\varphi_1 - \beta_1) = (r^2 + \ell_1^2 + \ell_2^2 - \ell_3^2 + 2 \ell_1 \ell_2 \cos \varphi_2)/(2 r b) \quad (27)$$

This equation has two solutions $\varphi_{1,I}$ and $\varphi_{1,II}$ for φ_1 . They are parametrically dependent on φ_2 . Now, let us compute the angle φ_3 . Equation (10) can be rewritten as follows

$$\begin{aligned} (r^2 - \ell_1^2 - \ell_2^2 - \ell_3^2 - 2 \ell_1 \ell_2 \cos \varphi_2)/(2 \ell_3) \\ = (\ell_1 \cos \varphi_2 + \ell_2) \cos \varphi_3 - \ell_1 \sin \varphi_2 \sin \varphi_3. \end{aligned} \quad (28)$$

Let us define another auxiliary variable β_2 , such that

$$\begin{aligned} \ell_1 \cos \varphi_2 + \ell_2 &= b \cos \beta_2 \\ \ell_1 \sin \varphi_2 &= b \sin \beta_2. \end{aligned} \quad (29)$$

Thus, as in the previous case, for $\varphi_2 \neq \pm\pi$, there exists only one unique angle β_2 , which can be computed from (29). If equations (29) are substituted into (28), the following condition can be written:

$$\cos(\varphi_3 + \alpha_2) = (r^2 - \ell_1^2 - \ell_2^2 - \ell_3^2 - 2 \ell_1 \ell_2 \cos \varphi_2)/(2 \ell_3 b). \quad (30)$$

Now, it is possible to compute two values $\varphi_{3,I}$ and $\varphi_{3,II}$, as it was mentioned in the previous section.

C. Computation of φ_1 and φ_2 as Functions of φ_3

Let us denote the expression in square brackets in (10) by the letter d . Thus, d can be easily expressed as:

$$\begin{aligned} d = \ell_1 [(\ell_2 + \ell_3 \cos \varphi_3) \cos \varphi_2 - \ell_3 \sin \varphi_3 \sin \varphi_2] \\ + \ell_2 \ell_3 \cos \varphi_3. \end{aligned} \quad (31)$$

In a similar way to the previous sections, let us define auxiliary variables $c \geq 0$ and γ_1 as follows:

$$\begin{aligned} \ell_3 \cos \varphi_3 + \ell_2 &= c \cos \gamma_1 \\ \ell_3 \sin \varphi_3 &= c \sin \gamma_1. \end{aligned} \quad (32)$$

From (32), the variable c is the following

$$c = \sqrt{\ell_2^2 + \ell_3^2 + 2 \ell_2 \ell_3 \cos \varphi_3}, \quad (33)$$

c is zero only for $\ell_2 = \ell_3$ and $\varphi_3 = \pi$. In our construction, $\ell_2 > \ell_3$ is assumed, so $c > 0$ always. Then, from (32):

$$\begin{aligned} \cos \gamma_1 &= (\ell_3 \cos \varphi_3 + \ell_2)/c \\ \sin \gamma_1 &= (\ell_3 \sin \varphi_3)/c. \end{aligned} \quad (34)$$

Thus, there exists only one unique angle γ_1 satisfying (34). Then, d from (31) can be rewritten as

$$d = \ell_1 [c \cos \gamma_1 \cos \varphi_2 - c \sin \gamma_1 \sin \varphi_2] + \ell_2 \ell_3 \cos \varphi_3.$$

or in compact form

$$d = \ell_1 c \cos(\varphi_2 + \gamma_1) + \ell_2 \ell_3 \cos \varphi_3 \quad (35)$$

Hence, relation (10) can be rewritten as:

$$r^2 = \ell_1^2 + \ell_2^2 + \ell_3^2 + 2 d. \quad (36)$$

From (35) and (36), let us compute

$$\cos(\varphi_2 + \gamma_1) = (r^2 - \ell_1^2 - \ell_2^2 - \ell_3^2 - 2 \ell_2 \ell_3 \cos \varphi_3)/(2 \ell_1 c). \quad (37)$$

In a similar way as in previous sections, two possible values for the angle φ_2 , i.e. $\varphi_{2,I}$ and $\varphi_{2,II}$, can be determined.

To determine the remaining angle φ_1 as a function of φ_3 , let us define in relation (13) the following expressions:

$$x = r \cos \gamma_2, \quad y = r \sin \gamma_2. \quad (38)$$

Considering (38), expression (13) has the form:

$$r^2 - 2\ell_1 r \cos(\varphi_1 - \gamma_2) = \ell_2^2 + \ell_3^2 - \ell_1^2 + 2\ell_2 \ell_3 \cos \varphi_3. \quad (39)$$

Hence, expression (39) may be rewritten as

$$\cos(\varphi_1 - \gamma_2) = \frac{r^2 + \ell_1^2 - \ell_2^2 - \ell_3^2 - 2\ell_2 \ell_3 \cos \varphi_3}{2\ell_1 r}. \quad (40)$$

This formula is valid since $r > 0$ holds always. In this case, angle γ_2 can be uniquely determined from equations (38). By analogy with the previous cases, we can determine two possible angles $\varphi_{1,I}$, $\varphi_{1,II}$. Both of these angles were calculated from the magnitude of angle φ_3 . This meets our task.

Note that after each calculation, the appropriate range of the angle should be adjusted to suit the technical requirements. For instance, if we ask for angles φ_i to be in the range $-\pi < \varphi_i < \pi$, it is necessary to perform the corresponding transformation.

VI. USE OF FIXED CONSTRAINTS BETWEEN VARIABLES

The previous procedure is actually one of the possible alternatives when we use some definite constraint $\varphi_i = \varphi_i(t)$ or $= \text{const.}$, i.e. over time, varying or constant in (1) $x = x(\varphi_1, \varphi_2, \varphi_3)$ and in (2) $y = y(\varphi_1, \varphi_2, \varphi_3)$. Generally, any additional constraint for the angles will be understood as an equation $g(\varphi_1, \varphi_2, \varphi_3) = 0$. Although, infinitely many equations can be written, their suitable selection with respect to application can accelerate the calculation.

For instance, let the angles φ_2, φ_3 be interdependent, but independent on the angle φ_1 . That is, arbitrary position of φ_1 can be achieved without any influence of a possible constraint $\bar{g}(\varphi_2, \varphi_3) = 0$. This constraint may be realized arbitrary in many ways. However, the simplest will be to use linear coupling. So let us ask for $\varphi_3 = k\varphi_2$ to be true. To minimize numerical calculation choose $k = \pm 1$.

A. Option $k = +1$

This option represents the equality requirement $\varphi_3 = \varphi_2$. If we substitute this requirement into (10), then

$$r^2 - \ell_1^2 - \ell_2^2 - \ell_3^2 = 2[\ell_1 \ell_2 \cos \varphi_2 + \ell_1 \ell_3 \cos(2\varphi_2) + \ell_2 \ell_3 \cos \varphi_2]. \quad (41)$$

Since $\cos(2\varphi_2) = 2\cos^2\varphi_2 - 1$, we can write (41) in the form

$$2\ell_1 \ell_3 \cos^2 \varphi_2 + \ell_2(\ell_1 + \ell_3) \cos \varphi_2 + \frac{1}{2}(\ell_1^2 + \ell_2^2 + \ell_3^2 - r^2) - \ell_1 \ell_3 = 0. \quad (42)$$

This quadratic equation has generally two solutions

$$\cos \varphi_2 = \frac{-\ell_2(\ell_1 + \ell_3) \pm \sqrt{D}}{4\ell_1 \ell_3}, \quad (43)$$

for $\cos \varphi_2$, where discriminant D is as follows

$$D = (\ell_1 - \ell_3)^2 (\ell_2^2 - 4\ell_1 \ell_3) + 4\ell_1 \ell_3 r^2. \quad (44)$$

Thus, in general, the one φ_2 has to be chosen from four possible values: quadratic function and an even function $\cos \varphi_2$.

TABLE II
THE POSSIBLE VARIANTS OF ANGLES $\varphi_{[2,3],[I,II]}$

I	II	III	IV
$\varphi_{2,I}$	$\varphi_{2,I}$	$\varphi_{2,II}$	$\varphi_{2,II}$
$\varphi_{3,I}$	$\varphi_{3,II}$	$\varphi_{3,I}$	$\varphi_{3,II}$

B. Option $k = -1$

This option represents the equality requirement $\varphi_3 = -\varphi_2$. If we substitute this requirement into (10), then

$$r^2 - \ell_1^2 - \ell_2^2 - \ell_3^2 = 2[\ell_2(\ell_1 + \ell_3) \cos \varphi_2 + \ell_1 \ell_3]. \quad (45)$$

However, from (45), we immediately obtain that

$$\cos \varphi_2 = \frac{r^2 - \ell_2^2 - (\ell_1 + \ell_3)^2}{2\ell_2(\ell_1 + \ell_3)}. \quad (46)$$

Generally, there are two possible values of the angle φ_2 . In both cases, the angle φ_3 is determined. Thus, (13) can be used, as in equations (38)–(40), to determine the angle φ_1 .

VII. TRAJECTORIES

The motion trajectories of the robot are known and given in advance according to building requirements, i.e. architectural design and construction documentation. The end link carrying printing head moves usually by constant velocity. Other links move to meet all requirements for the considered trajectory, especially needed robot configuration from print point of view, precision of print, velocity and acceleration of individual robot links etc. The procedure is quite usual. The predefined motion path is split into individual segments by a sequence of dividing points. In these points, the inverse task is solved considering given requirements. Individual cases will be presented on several special tasks:

- Options relating to III-B 1) —————
(Inverse kinematics and selected one angle)

A. Angle φ_1 as a Determining Parameter

Let angle φ_1 be some predetermined function, generating an appropriate varying parameter, and angles φ_2 and φ_3 be calculated. Parameter φ_1 can change, e.g. with a constant velocity, and have at the beginning and end a gradually increasing and decreasing velocity. The results from section V-A are used. The procedure is the following. Let a in (18) be calculated for the values of position x , y and joint angle φ_1 . Using (19) and (20), angle α is uniquely determined. Using (22), angle $\delta = \varphi_2 - \alpha$ is calculated. In general, there are two possible results δ_I and δ_{II} . Thus, angle φ_2 has two possible values: $\varphi_{2,I} = \alpha + \delta_I$ and $\varphi_{2,II} = \alpha + \delta_{II}$. Considering (23), there are two possible values $\varphi_{3,I}$ and $\varphi_{3,II}$.

Thus, in total, there are the following variants for choosing angles φ_2 and φ_3 in the Tab. II. For the initial point of the trajectory, the selection from variants I-IV is arbitrary. If some other requirements are preset, some variant in the Tab. II may not be sufficient.

Let angles φ_2 and φ_3 in some internal point of the trajectory have to be determined and some selection was already done in the previous point of the trajectory.

In the following searched point, the variant from I-IV is selected such that it is not only admissible (i.e. meets given constraints), but furthermore it meets the requirement of minimal distance against previous step. The distance can be suitably selected as a sum of absolute values of increments of the both angles φ_2 and φ_3 .

This task, when φ_1 is selected in advance as parameter and rest two angles φ_2 and φ_3 are calculated, has the following meaning and utilisation:

The sampling of the trajectory or time solution interval is provided. The angle φ_1 , in particular sampling points, is gradually changed, for instance, for the same constant $\Delta\varphi_1$, so that the angular speed of the first axis is constant or slightly varying. In each sampling instant, both angles φ_2 and φ_3 are calculated. If the first axis approaches its limit value, it is necessary to reduce its velocity or switch to different control strategy.

B. Supplement of φ_2 or φ_3 as an Optional Parameter

To solve the cases of requirement φ_2 or φ_3 as optional parameters, the procedure is in the analogy with the previous case. Instead of expressions in V-A, the another appropriate expressions in V-B for parameter selection φ_2 and in V-C for parameter selection φ_3 are used respectively.

- Options relating to III-B 2) _____
(Inverse kinematics and fixed mathematical constraint)

C. Requirement $\varphi_2 = \varphi_3$

For the requirement, when the last two angles have to be equal, i.e. $\varphi_2 = \varphi_3$, there is no parameter, see VI-A. A determining requirement is just relation $\varphi_2 = \varphi_3$.

In this case, both last rotational links tilt to the same side. The individual configurations of the robot arm look like a specific arc approximation by three linear segments, whose lengths are lengths of individual links of the arm.

The advantage is in the evenly tilting to the same side, e.g. for cases of specific obstacles in opposite side of the tilting. In addition, this option represents the arm motion with no big tilting of angles of individual links relatively to each other.

D. Requirement $\varphi_2 = -\varphi_3$

In this case, the third rotational link tilts on opposite side than the second one, see VI-B. It resembles a scissor mechanism. It is advantageous for a static balance of the whole robot arm and for the arm adjustment to the minimal transport volume.

Note that the last two requirements, described in the sections VII-C and VII-D, are usable for trajectories without any sharp turns. Such turns, i.e. singular points of the trajectory, are characterized by different derivatives from the left and right at a given break point. The case where such turns occur will be described in the following section VII-E.

- Option relating to III-B 1) (specific selection) _____
(Inverse kinematics, selected one angle, and x and y const.)

E. Requirement of Short Stay of the Robot End-Effector

At specific turning points, where a reference trajectory of the robot end-effector (TCP of the robot arm) has sharp break, the derivatives of the path geometry are not continuous, they differ from left and from right. In such points, the robot end-effector is stopped.

In the case of conventional robots, all links must be stopped in these points and the whole kinetic energy of the links is lost during braking and stopping. Such losses are useless. However, this situation may not occur for the construction proposed in this paper.

Let us consider that TCP of printing head is not at the admissible limit of the robot arm, but it lies in some internal point, in which has to stop. Since, the proposed robot arm has redundant number of links for positioning in horizontal plane, the such internal point changes to the center of rotation for a short time, but the rotational robot links 1, 2 and 3 may not to stop.

For instance, let us consider a smooth uniform changing velocity of angle φ_1 with initial and final values: $\dot{\varphi}_{1, \text{Init}}$ and $\dot{\varphi}_{1, \text{Fin}}$, respectively [27]. For a uniform change of velocity from the initial to final value, the following expression is applicable

$$\omega_1(\tau) = \dot{\varphi}_1(\tau) = \dot{\varphi}_{1, \text{Init}} + c_1 \tau \quad (47)$$

where τ is a variable that represents a transition time from the initial velocity $\dot{\varphi}_{1, \text{Init}}$ to final velocity $\dot{\varphi}_{1, \text{Fin}}$. The time relation of such transition can be written with constant c_1 , representing constant angular acceleration for $c_1 > 0$ or deceleration for $c_1 < 0$ or constant velocity for $c_1 = 0$, respectively. Thus, for angular position is applicable

$$\varphi_1(\tau) = \varphi_{1, \text{Init}} + \dot{\varphi}_{1, \text{Init}} \tau + \frac{1}{2} c_1 \tau^2 \quad (48)$$

Then, the expression of overall transition time from $\dot{\varphi}_{1, \text{Init}}$ to $\dot{\varphi}_{1, \text{Fin}}$ follows from (47) for $c_1 \neq 0$

$$\tau_C = \frac{\dot{\varphi}_{1, \text{Fin}} - \dot{\varphi}_{1, \text{Init}}}{c_1} \quad (49)$$

By insertion of τ_C into (48), the overall change of angle φ_1 for the transition can be determined. If the overall transient time is split in several subintervals, then sampling interval are obtained, in which angle value φ_1 can be determined according to (48) as well as values of angles φ_2 and φ_3 using solution VII-A. In such case, the trajectory segment is reduced into one unique point $[x, y]$ in which the task of VII-A is solved repeatedly in different sampling instants.

The advantage of the procedure is that kinetic energy of individual links of complete kinematic chain is changed slowly. Indicated continuous changing represents the drifting of conventional horizontal system with 2 DOF. The result is a smooth motion of individual robot links, at which the last rotational link turns for the short time instant around the point, above which the print head stopped. The angle selection can be given with respect to the motion trajectory - one example of the motion with various selection of parameters is shown in section IX, Fig. 6–Fig. 8.

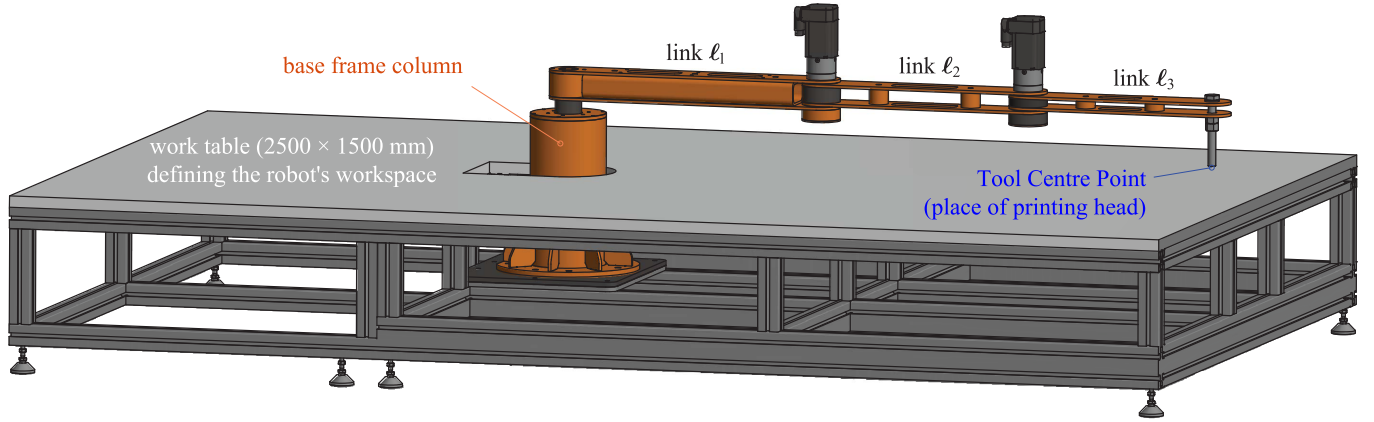


Fig. 3. CAD model of the proposed robot arm in scale 1 : 4.

VIII. SUPPLEMENT OF KINEMATICS

To complete the direct and inverse kinematic problem, in addition to the task of position described in V and VI, the tasks of velocities and accelerations remain to be solved. They will be explained in the following two subsections.

The solution will again follow the individual options of selected parameters and their corresponding time derivatives. The tasks of velocities and accelerations with already solved positions use Jacobian matrices that cover nonlinearities among used individual angular coordinates φ_1 , φ_2 and φ_3 .

A. Task of Velocities

Start with equations (1) and (2) in their general form:

$$\begin{bmatrix} x \\ y \end{bmatrix} = \begin{bmatrix} x(\varphi_1, \varphi_2, \varphi_3) \\ y(\varphi_1, \varphi_2, \varphi_3) \end{bmatrix}. \quad (50)$$

Then, *direct kinematics* for velocities is given as follows

$$\begin{bmatrix} \dot{x} \\ \dot{y} \end{bmatrix} = \begin{bmatrix} \frac{\partial x}{\partial \varphi_1} & \frac{\partial x}{\partial \varphi_2} & \frac{\partial x}{\partial \varphi_3} \\ \frac{\partial y}{\partial \varphi_1} & \frac{\partial y}{\partial \varphi_2} & \frac{\partial y}{\partial \varphi_3} \end{bmatrix} \begin{bmatrix} \dot{\varphi}_1 \\ \dot{\varphi}_2 \\ \dot{\varphi}_3 \end{bmatrix}, \quad (51)$$

$\underbrace{\quad}_{c_1} \quad \underbrace{\quad}_{c_2} \quad \underbrace{\quad}_{c_3}$

where individual columns c_1 , c_2 and c_3 are:

$$c_1 = \begin{bmatrix} -y \\ x \end{bmatrix}, \quad c_2 = \begin{bmatrix} \ell_1 \sin \varphi_1 - y \\ x - \ell_1 \cos \varphi_1 \end{bmatrix}, \quad c_3 = \begin{bmatrix} -\ell_3 \sin \psi_3 \\ \ell_3 \cos \psi_3 \end{bmatrix}, \quad (52)$$

with cumulative angle $\psi_3 = \varphi_1 + \varphi_2 + \varphi_3$, thus

$$\begin{bmatrix} \dot{x} \\ \dot{y} \end{bmatrix} = c_1 \dot{\varphi}_1 + c_2 \dot{\varphi}_2 + c_3 \dot{\varphi}_3. \quad (53)$$

The individual columns are $c_j = c_j(\varphi_1, \varphi_2, \varphi_3)$, $j = 1, 2, 3$. Then, *inverse kinematics* for the solved options, e.g. for φ_j , $j = 1, 2, 3$, from position task, and $\dot{\varphi}_1$ known parameter, is:

$$\begin{bmatrix} \dot{\varphi}_2 \\ \dot{\varphi}_3 \end{bmatrix} = [c_2 \ c_3]^{-1} ([\dot{x} \ \dot{y}]^T - c_1 \dot{\varphi}_1). \quad (54)$$

Matrix inversion is feasible if $\varphi_2 + \varphi_3 \neq k_1\pi \vee \varphi_1 + \alpha \neq \pi/2 + k_2\pi$, where $k_* \in \mathbb{Z}$, $\alpha \leftarrow x = r \sin \alpha$, $y = r \cos \alpha$. Some

column set leads always to inversion. The other options are solved for known velocities $\dot{\varphi}_2$ or $\dot{\varphi}_3$ and the same conditions.

Subsequent options with no angular parameter are:

$$k = +1 : g(\varphi_1, \varphi_2, \varphi_3) = \bar{g}(\varphi_2, \varphi_3) = \varphi_2 - \varphi_3 = 0$$

$$k = -1 : g(\varphi_1, \varphi_2, \varphi_3) = \bar{g}(\varphi_2, \varphi_3) = \varphi_2 + \varphi_3 = 0$$

These options are solved as follows

$$\begin{bmatrix} x \\ y \\ 0 \end{bmatrix} = \begin{bmatrix} x(\varphi_1, \varphi_2, \varphi_3) \\ y(\varphi_1, \varphi_2, \varphi_3) \\ g(\varphi_1, \varphi_2, \varphi_3) \end{bmatrix}, \quad J = \begin{bmatrix} \frac{\partial x}{\partial \varphi_1} & \frac{\partial x}{\partial \varphi_2} & \frac{\partial x}{\partial \varphi_3} \\ \frac{\partial y}{\partial \varphi_1} & \frac{\partial y}{\partial \varphi_2} & \frac{\partial y}{\partial \varphi_3} \\ \frac{\partial g}{\partial \varphi_1} & \frac{\partial g}{\partial \varphi_2} & \frac{\partial g}{\partial \varphi_3} \end{bmatrix}$$

$$\Rightarrow J = \begin{bmatrix} -y & \ell_1 \sin \varphi_1 - y & -\ell_3 \sin(\varphi_1 + \varphi_2 + \varphi_3) \\ x & x - \ell_1 \cos \varphi_1 & \ell_3 \cos(\varphi_1 + \varphi_2 + \varphi_3) \\ 0 & 1 & \pm 1 \end{bmatrix} \quad (55)$$

where signs ‘-’ and ‘+’ in (55) are for $k = +1$ and $k = -1$, respectively.

$$\begin{bmatrix} \dot{x} \\ \dot{y} \\ 0 \end{bmatrix} = J \begin{bmatrix} \dot{\varphi}_1 \\ \dot{\varphi}_2 \\ \dot{\varphi}_3 \end{bmatrix}, \quad \begin{bmatrix} \dot{\varphi}_1 \\ \dot{\varphi}_2 \\ \dot{\varphi}_3 \end{bmatrix} = J^{-1} \begin{bmatrix} \dot{x} \\ \dot{y} \\ 0 \end{bmatrix}. \quad (56)$$

B. Task of Accelerations

The *direct kinematics* for accelerations is defined:

$$\begin{bmatrix} \ddot{x} \\ \ddot{y} \end{bmatrix} = \dot{c}_1 \dot{\varphi}_1 + c_1 \ddot{\varphi}_1 + \dot{c}_2 \dot{\varphi}_2 + c_2 \ddot{\varphi}_2 + \dot{c}_3 \dot{\varphi}_3 + c_3 \ddot{\varphi}_3 \quad (57)$$

The corresponding *inverse kinematics* is as follows: for φ_i known from position task, $\dot{\varphi}_i$, $i = 1, 2, 3$, known from previous velocity task and $\ddot{\varphi}_1$ a known parameter:

$$\begin{bmatrix} \ddot{\varphi}_2 \\ \ddot{\varphi}_3 \end{bmatrix} = [c_2 \ c_3]^{-1} ([\ddot{x} \ \ddot{y}]^T - \dot{c}_1 \dot{\varphi}_1 - c_1 \ddot{\varphi}_1 - \dot{c}_2 \dot{\varphi}_2 - \dot{c}_3 \dot{\varphi}_3). \quad (58)$$

The other options can be solved similarly for known angular accelerations $\ddot{\varphi}_2$ and $\ddot{\varphi}_3$. Finally, options $k = \pm 1$ are solved as time derivatives of (56).

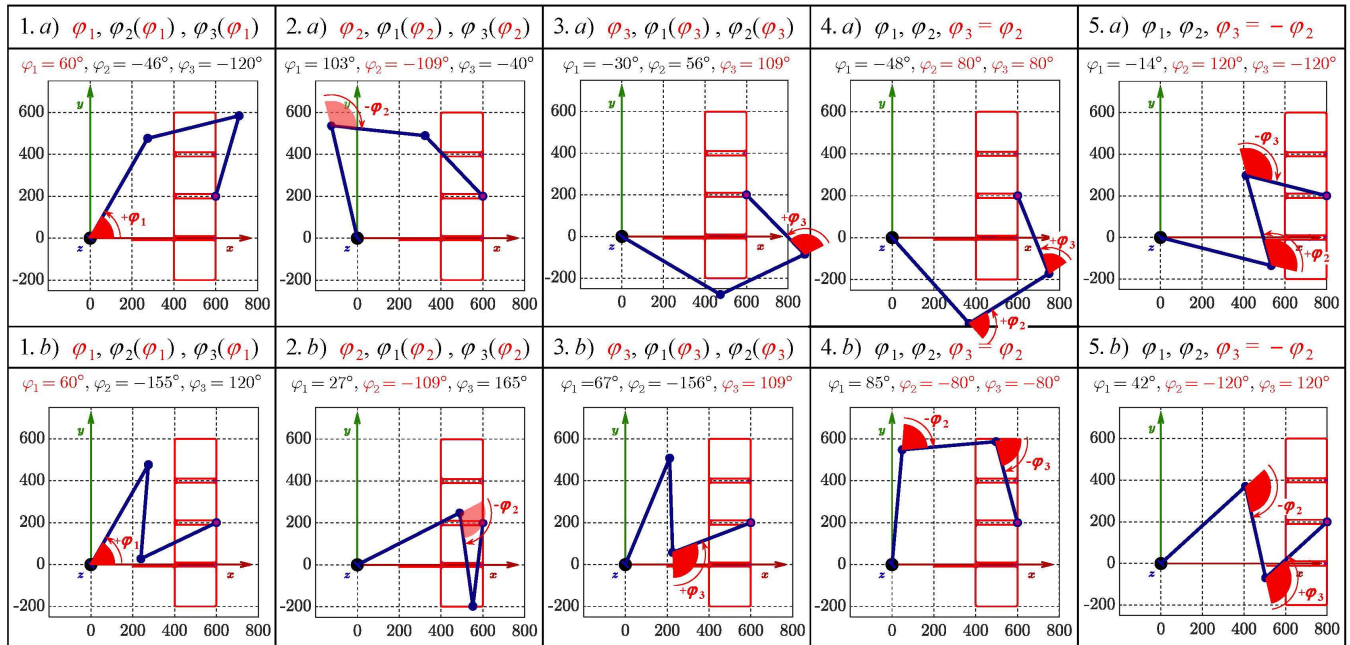


Fig. 4. XY views for given constraints (columns) and variants (rows) due to even function cosine in specific end-effector point.

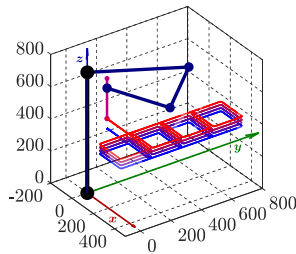


Fig. 5. 3D view of the motion trajectory from Fig. 4.

IX. SOLVED EXAMPLES

This section illustrates the derived theoretical outcomes using robot arm with design dimensions $\ell_1 = 2200$ mm, $\ell_2 = 1800$ mm, $\ell_3 = 1600$ mm, or its model in scale 1 : 4 with the corresponding lengths of the individual links $\ell_1 = 550$ mm, $\ell_2 = 450$ mm, $\ell_3 = 400$ mm, see Fig. 3. This figure shows a 3D CAD model of robot realisation.

A. Simulation Examples

The initial examples in Fig. 4 and Fig. 5 show robot configurations for the solved constraints for variants a) and b) relative to an even function cosine occurred in the derived expressions. The red highlighting indicates the angle as the selected parameter or the relation of angles φ_2 and φ_3 .

The options of the constraints in the variants a) and b) are:

1. φ_1 is the parameter, see section V-A;
2. φ_2 is the parameter, see section V-B;
3. φ_3 is the parameter, see section V-C;
4. $\varphi_3 = +\varphi_2$, see section VI-A;
5. $\varphi_3 = -\varphi_2$, see section VI-B.

In Fig. 4, note that the setting of one of the angles, φ_2 or φ_3 as the parameter, transforms the proposed robotic arm into usual SCARA form, but with the property of adjustable arm lengths. The connection of the two side points of the particular

arm couple (ℓ_1 and ℓ_2 or ℓ_2 and ℓ_3) forming the selected angle represents a specific artificial arm, length of which can be adjusted. However, this feature is not available with the SCARA robot. It may be useful, if the robot arm has to reach some positions in a constrained space such as positions around sharp corners, behind the obstacles or construction buttresses according to architectural or builder's requirements.

Furthermore, as it was already mentioned in section VII, the selection of φ_1 as a parameter represents a specific drifting motion of the conventional horizontal system with 2 DOF and a specific workspace extension with efficient energy distribution: keeping one level of potential energy, balanced kinetic energy and dynamic behavior in one horizontal layer at continuous constant changing of φ_1 .

The another example employs a testing trajectory in Fig. 6 that includes the two, separate lines and three sides of the equilateral triangle, i.e. in total five linear segments. Its geometry in Cartesian coordinates $[x, y, z]$ is given as:

- start in the initial point $[1400, 0, 500]$ mm;
- continuation by the three vertices of the triangle:
 1. vertex $[800 + 400 \sin(\frac{2}{3}\pi), 0, 500]$ mm,
 2. vertex $[800, 200, 500]$ mm,
 3. vertex $[800, -200, 500]$ mm,
 1. vertex $[800 + 400 \sin(\frac{2}{3}\pi), 0, 500]$ mm;
- return to the initial point $[1400, 0, 500]$ mm.

This example demonstrates the dwell of a robot end-effector in specific turning points, the vertices of the motion, with possible continuous steady motions of actuated joints. In these points, Cartesian coordinates x and y are fixed (constant). Thus, even though the printing head is stopped, the robot links may still move due to the additional 1 DOF – see section V.

However, if any mathematical constraint from section VI is activated, then the additional 1 DOF is exploited and robot would have to stop. In such cases, in some vicinity around the sharp turning point and inside (see red and orange

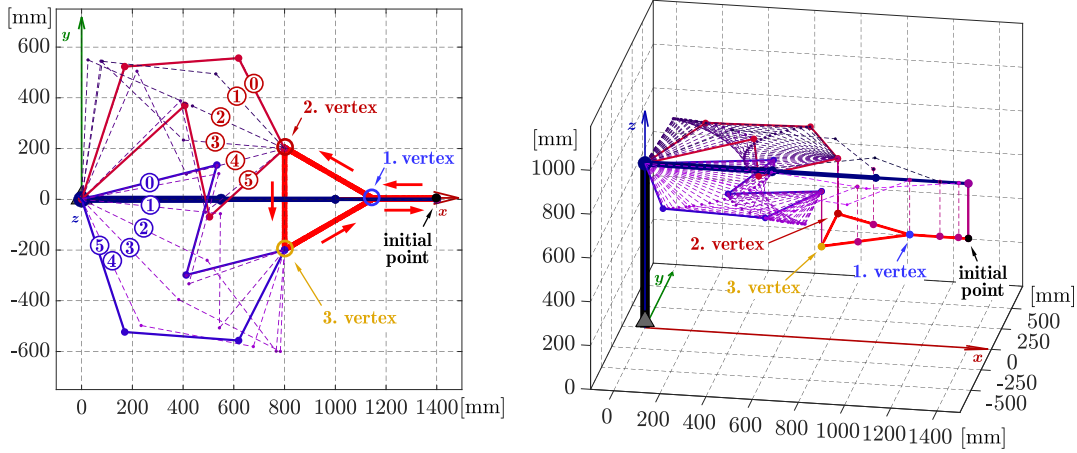


Fig. 6. Top view (left) and 3D view (right) of the robot motion with the arm reconfigurations.

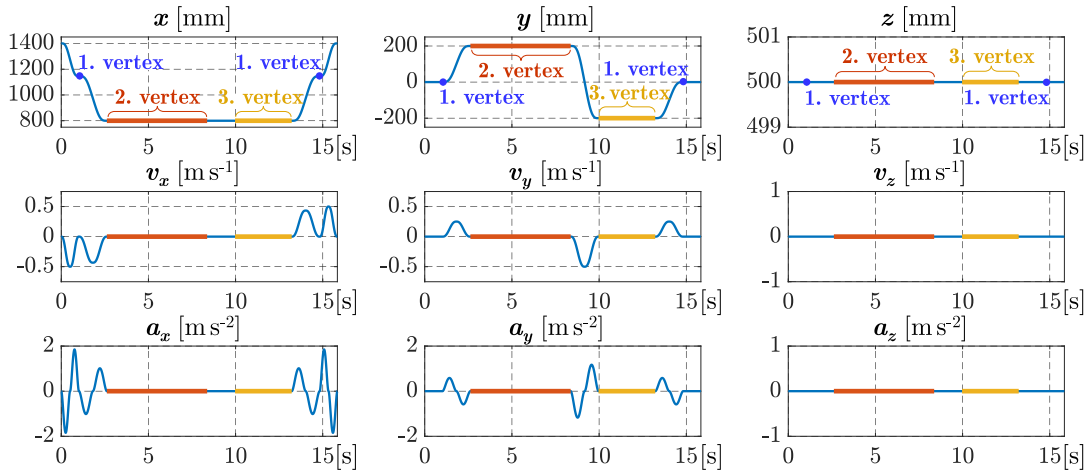


Fig. 7. Kinematic quantities: Cartesian coordinates and respective velocities and accelerations of robot end-effector for the motion shown in Fig. 6.

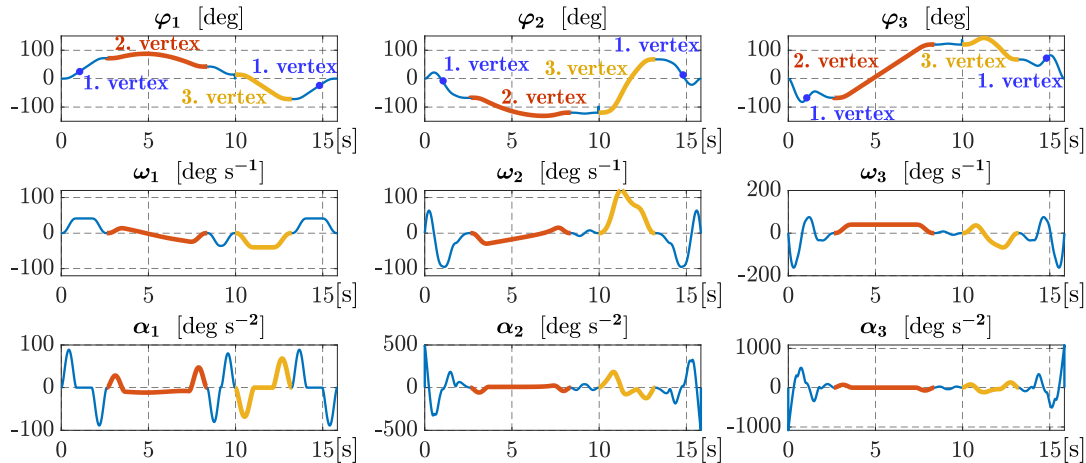


Fig. 8. Kinematic quantities: angular coordinates and respective velocities and accelerations of robot joints for the robot motion shown in Fig. 6.

circles in Fig. 6), the robot must be reconfigured by some aforementioned way from section V – see reconfiguration in 2. and 3. vertices in Fig. 6 (left side), where the motion is depicted in several selected phases for each sharp turn in top view (left side) and in 3D view (right side). The phase positions are indicated by numbers 0–5 in top view.

Time behaviors of kinematic quantities for the model 1 : 4 is depicted for Cartesian coordinates of the robot end-effector



Fig. 9. Realized laboratory model of robot arm in scale 1:4.

solutions of various structural constraints for added excess link that increases dexterity of the robot arm. Unlike usual approach based on Denavit-Hartenberg notation [23], the proposed representation in complex plane is more computationally efficient.

In the solution of inverse kinematic problem, the determination of the searched joint angles φ_1 , φ_2 and φ_3 as the optimisation problem was mentioned. For instance, the criterion with quadratic function can be given as follows

$$\min_{\dot{\varphi}_j} J \min_{\varphi_j} \int_0^{\tau} \sum_{j=1}^3 k_j (\dot{\varphi}_j)^2 dt \text{ subject to (1) and (2).} \quad (59)$$

The minimisation of (59) represents a classic variational problem with Lagrange multipliers [30]. It leads to the minimal angular velocities and determination of angles φ_1 , φ_2 and φ_3 . As the optimisation does not consider architectural requirements point of view and brings different calculus.

The proposed analytical solution in sections IV, V and VI, with supplement VII, is helpful for efficient trajectory planning and centralized model-based control design. Future work is focused on the synthesis of suitable models of dynamics for the model-based control design of realized laboratory model, which is now controlled by PID cascade control [31].

REFERENCES

- [1] P. Cascone, M. Laddaga, and F. Forestiero, "Digital construction: 3D printing for performative houses," in *Proc. 2nd RILEM Int. Conf. Concrete Digit. Fabr.* Cham, Switzerland: Springer, 2020, pp. 804–813.
- [2] P. Cascone, F. Galdi, A. Giglio, and E. Ciancio, "Architectural self-fabrication," *Int. J. Parallel, Emergent Distrib. Syst.*, vol. 32, no. sup1, pp. S39–S53, Dec. 2017.
- [3] R. Mathur, "3D printing in architecture," *Int. J. Innov. Sci., Eng. Technol.*, vol. 3, no. 7, pp. 2348–7968, 2016.
- [4] T. Wangler *et al.*, "Digital concrete: Opportunities and challenges," *RILEM Tech. Lett.*, vol. 1, pp. 67–75, Oct. 2016.
- [5] Y. W. D. Tay, M. Y. Li, and M. J. Tan, "Effect of printing parameters in 3D concrete printing: Printing region and support structures," *J. Mater. Process. Technol.*, vol. 271, pp. 261–270, Sep. 2019.
- [6] P. Sven, T. Dorn, M. Hirsch, C. Ehm, D. Stephan, and D. Vassiliadis, "Architectural applications and workflows for additive fabrication with concrete," in *Proc. 2nd RILEM Int. Conf. Concrete Digit. Fabr.* Cham, Switzerland: Springer, 2020, pp. 946–955.
- [7] V. Zada and K. Belda, "Application of Hamiltonian mechanics to control design for industrial robotic manipulators," in *Proc. 22nd Int. Conf. Methods Models Autom. Robot. (MMAR)*, Aug. 2017, pp. 390–395.
- [8] O. Geneidy, S. Kumarji, A. Dubor, and A. Sollazzo, "Simultaneous reinforcement of concrete while 3D printing," in *Proc. 2nd RILEM Int. Conf. Concrete Digit. Fabr.* Cham, Switzerland: Springer, 2020, pp. 895–905.
- [9] O. Lakhal, T. Chettibi, A. Belarouci, G. Dherbomez, and R. Merzouki, "Robotized additive manufacturing of funicular architectural geometries based on building materials," *IEEE/ASME Trans. Mechatronics*, vol. 25, no. 5, pp. 2387–2397, Oct. 2020.
- [10] 3DR HOLDINGS, LLC. *3DPRINT.COM Website*. Accessed: Aug. 20, 2020. [Online]. Available: <https://3dprint.com/google-search/?q=3D+concrete+printers>
- [11] 3DPrinthuset. (2017). *Cobod*. [Online]. Available: <https://cobod.com/>
- [12] 3DPrinthuset. (2018). *The BOD—Building On Demand*. Copenhagen, Denmark. [Online]. Available: <https://3dprinthuset.dk/The-BOD/>
- [13] A. Rudenko. (2014). *3D Concrete House Printer*. Minnesota. [Online]. Available: <http://www.totalkustom.com/>
- [14] H. S. An, T. W. Seo, and J. W. Lee, "Generalized solution for a sub-problem of inverse kinematics based on product of exponential formula," *J. Mech. Sci. Technol.*, vol. 32, no. 5, pp. 2299–2307, May 2018.
- [15] B. Kenwright, "Inverse kinematics with dual-quaternions, exponential-maps, and joint limits," *Int. J. Adv. Intell. Syst.*, vol. 6, nos. 1–2, pp. 53–65, 2013.
- [16] R. Yi, C. Wu, Y.-J. Liu, Y. He, and C. C. L. Wang, "Delta DLP 3-D printing of large models," *IEEE Trans. Autom. Sci. Eng.*, vol. 15, no. 3, pp. 1193–1204, Jul. 2018.
- [17] C. Urrea and J. Kern, "Modeling, simulation and control of a redundant SCARA-type manipulator robot," *Int. J. Adv. Robot. Syst.*, vol. 9, no. 2, pp. 1–14, 2012.
- [18] J. Wanner and O. Sawodny, "Tool-center-point control of a concrete pump using constrained quadratic optimization," *IEEE Trans. Autom. Sci. Eng.*, vol. 18, no. 1, pp. 382–396, Jan. 2021.
- [19] R. C. Luo and Y. W. Perng, "Adaptive skew force free model-based synchronous control and tool center point calibration for a hybrid 6-DoF gantry-robot machine," *IEEE/ASME Trans. Mechatronics*, vol. 25, no. 2, pp. 964–976, Apr. 2020.
- [20] M. A. Houran, X. Yang, and W. Chen, "Two-degree-of-freedom WPT system using cylindrical-joint structure for applications with movable parts," *IEEE Trans. Circuits Syst. II, Exp. Briefs*, vol. 68, no. 1, pp. 366–370, Jan. 2021.
- [21] G. Niu, B. Pan, Y. Fu, and C. Qu, "Development of a new medical robot system for minimally invasive surgery," *IEEE Access*, vol. 8, pp. 144136–144155, 2020.
- [22] B. Huang, Y. Yang, Y.-Y. Tsai, and G.-Z. Yang, "A reconfigurable multirobot cooperation workcell for personalized manufacturing," *IEEE Trans. Autom. Sci. Eng.*, early access, Aug. 4, 2021, doi: 10.1109/TASE.2021.3092560.
- [23] Y. He *et al.*, "Dynamic modeling, simulation, and experimental verification of a wafer handling SCARA robot with decoupling servo control," *IEEE Access*, vol. 7, pp. 47143–47153, 2019.
- [24] W. Rudin, *Real and Complex Analysis*. New York, NY, USA: McGraw-Hill, 1986.
- [25] K. Rektorys *et al.*, *Survey of Applicable Mathematics*. New York, NY, USA: Springer, 1994.
- [26] V. Záda and K. Belda, "Mathematical modeling of industrial robots based on Hamiltonian mechanics," in *Proc. 17th Int. Carpathian Control Conf. (ICCC)*, May/Jun. 2016, pp. 813–818.
- [27] B. Siciliano and O. Khatib, Eds., *Handbook Robotics*. Heidelberg, Germany: Springer, 2008.
- [28] B&R. *Motion Ctrl/ACOPOS P3*. Accessed: Jul. 30, 2021. [Online]. Available: <https://www.br-automation.com/en/products/motion-control/acopos-p3/>
- [29] B&R. *Motion Ctrl/8LVB Motors*. Accessed: Jul. 30, 2021. [Online]. Available: <https://www.br-automation.com/en/products/motion-control/8lvb-gear-motors/>
- [30] D. Kirk, *Optimal Control Theory*. New York, NY, USA: Dover, 1998.
- [31] TU, Liberec. *3D Star*. Accessed: May 22, 2020. [Online]. Available: <http://3dstar.tul.cz/en>



Václav Záda received the M.Sc. degree in automation and the Ph.D. degree in technical cybernetics from Czech Technical University in Prague in 1981 and 1987, respectively, and the M.Sc. degree in theoretical cybernetics and mathematical structures from Charles University, Prague, Czech Republic, in 1994. Since 1997, he has been a Senior Lecturer with the Technical University of Liberec. His research interests include mathematical logic and structures, functional analysis, and control theory.



Květoslav Belda received the M.Sc. degree in automatic control and engineering informatics and the Ph.D. degrees in technical cybernetics and in electrical engineering and informatics from Czech Technical University in Prague, in 1999, 2003, and 2006, respectively. Since 1999, he has been a Researcher with the Institute of Information Theory and Automation, Czech Academy of Sciences. His research interests include model-based control design and industrial robotics.